Modeling of electroabsorption in semiconductor quantum structures within the eight-band k·p theory

Mats-Erik Pistol* and David Gershoni

Department of Physics and Solid State Institute, Technion-Israel Institute of Technology, Haifa 32000, Israel
(Received 21 March 1994)

We have incorporated electric fields into the eight-band k·p theory, which we have applied to hetero-structures, in conjunction with the envelope-function approximation. We use the method of Baraff and Gershoni to implement the electric-field effects in a computer program that calculates the optical properties of direct-band-gap heterostructures in one, two, and three dimensions. Using this method, we calculate the interband and intersubband electroabsorption of multiple quantum wells as well as the inter-band electroabsorption in superlattices. We illustrate the evolution of the Stark localization of the electron wave function under the application of an external electric field in superlattices. Comparison with experimental data, available in the literature, exhibits very good agreement between theory and experiment, with respect to the spectral shape, the absolute magnitude, and the electric-field dependence of the absorption.

I. INTRODUCTION

The electronic and optical properties of semiconductor quantum wells (QW's) and superlattices (SL's) is a subject of great interest for both fundamental and applied research. In particular, the properties of heterostructures in the presence of an applied electric field perpendicular to the interfaces have been studied.[1] The electric field induces a pronounced redshift of the heavy-hole exciton resonance, while the quantum confinement prevents the dissociation of the exciton and maintains a well-defined resonance. This effect, also known as the quantum confined Stark effect[1,2] (QCSE), has been investigated by means of photoluminescence (PL),[3] time-resolved PL,[4] PL excitation,[5] photocurrent,[6] and direct absorption due to both interband[7] and intersubband[8] transitions.

This interest in the QCSE is strongly motivated by its applications in a variety of electro-optic devices such as modulators,[9] wavelength selective detectors,[10] optically bistable switches,[11] and others.[12] Thus, a need for an accurate model for the electroabsorption properties of QW's and SL's exists not only on a pure scientific ground, but also as an important engineering tool.

The eight-band k·p method, as formulated by Kane,[13] is remarkably successful in describing the electronic and optical properties of diamond and zinc-blende bulk lattices. This method allows for an empirical determination of the structure of the electronic bands that are closest to the fundamental band gap. In order to make this determination, parameters such as band gaps and effective masses are needed. These can be measured with a high degree of accuracy. Together with the envelope-function approximation,[14] this method forms a powerful tool for modeling the optical and electronic behavior of the most technologically important *intrinsic and extrinsic* bulk semiconductors. Eppenga, Schuurmans, and Colak showed that this method works as well for the description of the optical properties of QW's realized in these bulk semiconductors.[15] Using a Fourier expansion of the eight-band envelope functions, and thus bypassing the difficulty in matching conditions on each internal interface, Baraff and Gershoni (BG) have formulated a method for modeling quantum structures and superlattices in several dimensions.[16] Their method and approach are unique in that they provide one general method for calculating the absorption of bulk semiconductor, one-dimensional QW SL's and multiple quantum wells (MQW's), two-dimensional quantum systems such as quantum wires, and three-dimensional systems such as quantum dots. For all of these systems an equally simple means of modeling the optical transitions across the fundamental band gap (interband transitions), as well as transitions between sublevels within the conduction band and within the valence band (intersubband transitions), are provided.[17]

In this paper, we generalize the BG method to include electric fields. We show that the inclusion of electric fields is straightforward and does not result in any increase in computer requirements. The scope of this paper is the following. In Sec. II we briefly outline the theory and the approximations involved in the modeling. In Sec. III we compare our calculations with experimental data from the literature. Our model is applied for modeling the QCSE in MQW's and the formation of a Stark ladder in a SL. We conclude by calculating the QCSE in transitions within the conduction band. A short summary is presented in Sec. IV.

II. THEORY

The single-particle electronic-energy eigenvalues and eigenfunctions in a periodic semiconductor system are given by the solutions of the Schrödinger equation:

$$H\Psi = [p^2/2m_0 + V(\mathbf{r})]\Psi(\mathbf{r}) = E\Psi(\mathbf{r}) , \qquad (1)$$

where H is the Hamiltonian, $\Psi(\mathbf{r})$ is the wave function of the electron, E is its energy, m_0 is its mass, $\mathbf{p}$ is its momentum operator, $\mathbf{r}$ is its position vector, and $V(\mathbf{r})$ is

the potential in which it moves. In the effective-mass approximation, the wave function is expressed as a sum over zone-center Bloch functions $u_{j0}(\mathbf{r})$,

$$\Psi(\mathbf{r}) = \sum_j F_j(\mathbf{r})u_{j0}(\mathbf{r}) , \qquad (2)$$

where $F_j(\mathbf{r})$ are called envelope functions. Throughout this paper the sum in Eq. (2) runs over the eight bands closest to the fundamental gap. More specifically, we consider only two conduction-band Bloch functions denoted by $|s,\uparrow\rangle$ and $|s,\downarrow\rangle$, and six valence-band Bloch functions denoted by $|x,\uparrow\rangle$, $|x,\downarrow\rangle$, $|y,\uparrow\rangle$, $|y,\downarrow\rangle$, $|z,\uparrow\rangle$, and $|z,\downarrow\rangle$, respectively. The functions are named according to their symmetry and spin properties.[13] The Schrödinger equation for a homogeneous bulk semiconductor is now given by a set of eight coupled equations:

$$\sum_i H_{ji}(\mathbf{k})F_i(\mathbf{r}) = E(\mathbf{k})F_j(\mathbf{r}) , \qquad (3)$$

where $H_{ji}(\mathbf{k})$, are the matrix elements of the Hamiltonian in this approximation and k is the electron wave vector. Following Kane,[13] a second order in $\mathbf{k}$ perturbation expansion is used to obtain the matrix elements $H_{ji}(\mathbf{k})$. Thus the solution to Eq. (3) yields the band structure of the bulk material near the Brillouin-zone center ($\mathbf{k}=0$). The parameters in the matrix element, $H_{ji}(\mathbf{k})$, can thus be obtained from comparison with experiments or with other methods of band-structure calculations. The generalization of Eq. (3) to include strain has recently been carried out by Bahder,[18] extending previous work by Pikus and Bir.[19]

In order to include an externally applied electric field, Eq. (3) has to be modified slightly. The modification affects only the diagonal matrix elements of Eq. (3). This can be accomplished if one uses the prescription[14] that in the presence of external fields, which are described by a vector potential $\mathbf{A}$ and a scalar potential ϕ, the wave vector $\mathbf{k}$ in Eq. (3) is replaced by $\mathbf{k}-(e/c)\mathbf{A}$, and the energy E is replaced by $E-\phi$. The latter replacement is not mentioned in Ref. 14, but can be arrived at, in a straightforward manner, if one treats the scalar potential as the fourth component of the covariant four-vector $\mathbf{A}$. These replacements are similar to the prescription for constructing the Hamiltonian for a free electron in an external electromagnetic field.[20] The conclusion that the electric field affects only the diagonal terms of the effective Hamiltonian was used before us in four- and six-band models.[21]

When using Eq. (3) to obtain the band structure of a bulk semiconductor close to the Brillouin-zone center, the crystal momentum $\mathbf{k}$ is interpreted as a label to the Bloch wave functions. Equation (3) can also be used to solve a heterostructure problem, in which case $\mathbf{k}$ is interpreted as the differential operator $(1/i)\nabla$. The resulting matrix equation becomes

$$\sum_i H_{ji}(r,\nabla)F_i(\mathbf{r}) = EF_j(\mathbf{r}) . \qquad (4)$$

In the BG method the functions $F_j(\mathbf{r})$ are expanded using

plane waves and the resulting matrix equation is solved, as described in Ref. 16. The problem of wave-function matching at the interfaces is solved by using surface integrals, instead of using a more cumbersome algebraic approach. All of the integrals that are needed in the calculation of the matrix elements are evaluated analytically, making the method highly efficient.

In our implementation, we assume piecewise constant electric fields along the Cartesian axes. These are defined by the confining potentials, and do not, necessarily, coincide with the crystallographic axes. In two or three dimensions, corresponding to quantum wires and quantum dots, the electric field is specified by its components along the Cartesian axes and may, therefore, not be chosen independently for each region. It is, in fact, not possible to include arbitrary fields within each material region without violating Maxwell's equations. If arbitrary electric fields are included in each region, the problem must be solved self-consistently. This would modify the electric fields. For the time being, self-consistency is not included in our calculations. Thus, our calculations yield accurate results only for relatively low concentrations of charge carriers (typically below 1×10^{17} cm^{-3}).

The model, which uses a discrete Fourier expansion of the envelope functions, requires a periodic-potential structure in each direction. Thus, in addition to the structural periodicity of the quantum structure, the electrostatic potential should also be periodic. For this purpose, we introduce an electric field into one of the regions of our unit cell, in such a way that the potential drop over the entire unit cell is zero. The region into which this "fake" field is introduced is chosen so that it does not affect the calculated electroabsorption. Figure 1 illustrates the potential structure in a typical simulation of a superlattice under an applied electric field. The interesting region (four quantum wells in Fig. 1) denoted by C is situated between barriers A, which have unrealistically high potentials in order to prevent coupling effects with neighboring unit cells. Additional cladding layers B are sometimes introduced in the calculated structure to minimize edge effects caused by the introduction of the isolating barriers A. These barriers do not affect the spectrum at the range of interest, thus the corresponding electric
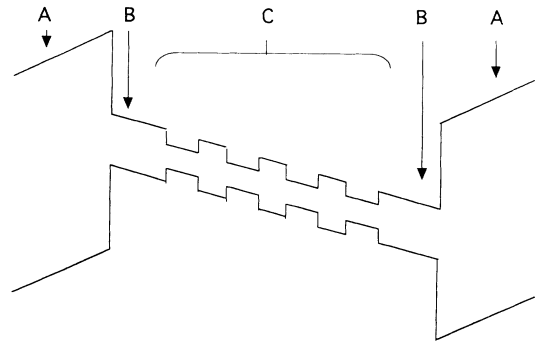

FIG. 1. A typical potential structure used for simulations. The electroabsorption is calculated only for the part of the structure that is denoted by C.

field can be chosen at will. It is chosen such that the total potential drop across the entire unit cell is zero.

We will now describe three different effects we have calculated: (i) the Stark effect in multiple quantum wells, (ii) the formation of Stark ladders in an $Al_xGa_{1-x}As/GaAs$ superlattice, and (iii) the Stark effects on interconduction subband transitions. These examples have been chosen in part to establish the validity and accuracy of our method and in part to illustrate the range of properties that may be calculated using the same unified method.

III. COMPARISON WITH EXPERIMENTS

A. Stark effect in unstrained quantum wells

We have used the method to compare our calculations with the measured electroabsorption spectra of Bar-Joseph et al.[22] Their structure consisted of a superlattice of alternating InP barriers and lattice matched $In_xGa_{1-x}As$ quantum wells, each 100 Å thick. The absorption was measured at normal incidence, i.e., the light propagated parallel to the growth direction and was polarized parallel to the QW planes (TE polarization). Figure 2 shows the measured and computed absorption spectra at zero electric field and at a field of 150 kV/cm. The computed spectra have been rigidly shifted 10 meV towards lower energy in order to partially account for the binding energy of the excitons. The input structure to the computer program was similar to that shown in Fig. 1. In order to reduce the unit-cell length, we used in this case only three QW's in a cell. This, in turn, reduces the number of plane waves required in the Fourier expansion of the envelope functions and shortens the computing time considerably. We found that for states close to the QW band edges it is often sufficient to use a single quantum well in the simulated unit cell. This is not the case for higher-energy states, where a substantial overlap between the wave functions of adjacent wells occurs. Here, it is necessary to use several quantum wells. The number of QW's needed were found by a simple convergence test of the calculated spectrum at the energy range of interest. For the calculation of Fig. 2(b) we found full convergence using 41 plane waves, giving a computing time of about 1 h on a modern workstation.

As may be guessed from the diagram of the potential shown in Fig. 1 the lowest-energy electron states are "pulled" by the electric field to the right and tend to concentrate in the right corner of the right region B. In contrast, the highest-energy valence-band states tend to concentrate in the left corner of the left region B. These states, which result from the introduction of the isolating barrier A, do not describe the experimental situation realistically. Fortunately, their overlap is negligible and they contribute very little to the calculated absorption (more than three orders of magnitude less than the absorption from states localized in the same wells). However, increasing the number of wells in the unit cell has a computational disadvantage. It forces us to consider many states covering a large range of energies from the lowest-energy states, which contribute very little to the
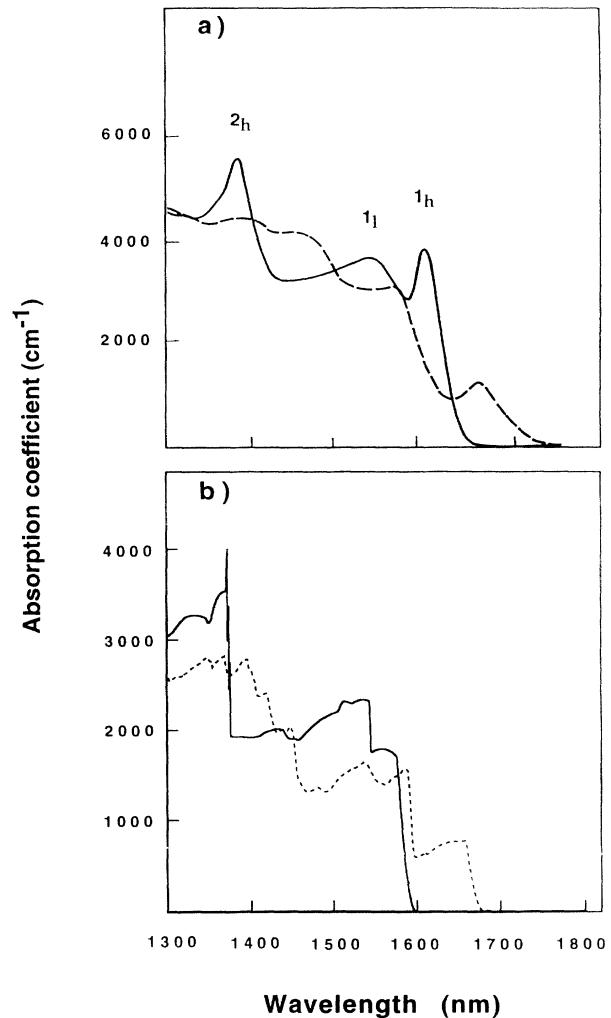

FIG. 2. Experimentally (a) and computed (b) absorption spectra of the $In_xGa_{1-x}As/InP$ MQW at electric fields of 0 kV/cm (solid line) and 150 kV/cm (dashed line). The experimental data are from Ref. 23.

absorption, to the relevant higher-energy states, which do contribute to the absorption. In the calculations, results given in Fig. 2(b), we had to consider 24 conduction-band states and 46 valence-band states before convergence was achieved. At normal incidence the electromagnetic radiation fields are polarized parallel to the superlattice planes (TE). At this polarization, the heavy-hole to conduction-band transitions at zero in-plane wave vector are allowed and are, approximately, three times stronger than the corresponding transitions from the light-hole bands.[23] Without an applied electric field three spectral features are observed in the experimental absorption spectrum [displayed by the solid line in Fig. 2(a)]. These features, at energies of 0.77 eV (denoted 1_h in the figure), 0.80 eV (denoted 1_l), and 0.89 eV (denoted 2_h), are identified as the highest heavy-hole band (HH1) to the lowest electron-band (EL1) transition, the highest light-hole band (LH1) to EL1 transition, which is overlapping with the second heavy-hole band (HH2) to EL1 transi-

tion, and finally the second heavy-hole band (HH2) to the second electron-band (EL2) transition, respectively. The calculated spectrum [described by the solid line in Fig. 2(b)], shows the same features and is generally similar in shape to the experimental one. There is, however, one prominent difference between the two spectra. The calculated HH1 to EL1 transition does not, in spectral shape, resemble the enhanced resonance observed at this transition energy. This is expected, since our model ignores the excitonic effect, which is known to be important for near-band-gap optical transitions of QW's even at room temperature.[24] It is, thus, surprising that our model describes the LH1-EL1 and HH2-EL2 transitions correctly. In particular, the observed enhancement of the latter transition is described quite accurately according to our calculations. We thus conclude that, at room temperature, excitonic effects are only important for the transition that is closest to the band edge. The enhancements observed for the higher-energy transition are more probably due to poles in the joint density of states. When a strong transverse electric field (150 kV/cm) is applied to the superlattice, the absorption spectrum undergoes a considerable change [dashed line, Fig. 2(a)]. The absorption edge shifts towards lower energy, the peaks get wider and the magnitude of the absorption at the edge is sharply reduced. The latter is intuitively expected since the lowest-energy electron (EL1) and the highest-energy hole (HH1) wave function will localize at different sides of the QW's. In this case, our simulations [Fig. 2(b), dashed line] provide a good description of the lowest HH1 to EL1 transition and of the almost complete disappearance of the HH2 to EL2 transitions. We thus conclude (unlike the authors of Ref. 22) that at these conditions even the lowest-energy exciton is completely destroyed by the electric field.

There are some differences between the calculated and the measured spectra. In the calculated spectrum, the LH1 to EL1 transition, which peaks at around 0.77 eV, seems to be double under the influence of an electric field. This is reasonable since this peak (at zero electric field) also corresponds to the normally forbidden HH2 to EL1 transition (see Fig. 3), which becomes allowed with electric field. This effect is not observed experimentally. We do not know the reason for this discrepancy. In addition, the absolute magnitude of the calculated absorption is roughly 30% less than the magnitude of the measured absorption. We do not feel that this is an indication of a problem with the computational method, as it is difficult to obtain an accurate determination of the absolute strength of the measured absorption. We consider the agreement to be very good.

In order to calculate the absorption spectrum, one needs to know the dispersion curves of carriers in the simulated quantum structure. The valence-band dispersion used for the calculations whose results are shown in Fig. 2(a) (no electric field) and Fig. 2(b) (150 keV/cm) is shown in Figs. 3(a) and 3(b), respectively. In Fig. 3(a) each dispersion curve is degenerate four times. For each energy there are four degenerate states having wave vectors and spins, which differ only in sign. This is due to the time-reversal and inversion symmetry of the effective
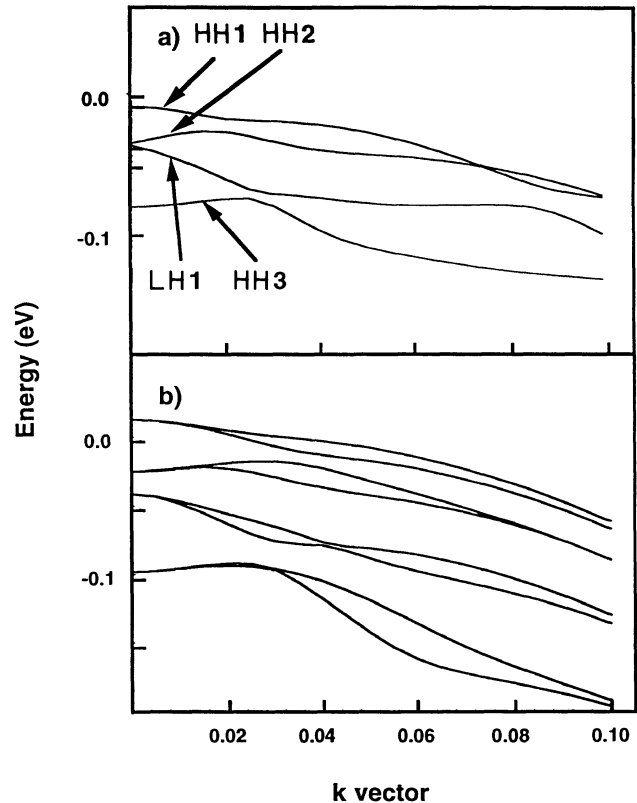

FIG. 3. The calculated valence-band structure of the $In_xGa_{1-x}As/InP$ MQW subject to an applied electric field of 0 (a) and 150 kV/cm (b).

Hamiltonian. (We neglect the small inversion asymmetry of the III-V compounds.[13]) The application of an external electric field breaks the inversion symmetry and only the Kramers degeneracy, which is associated with the time-reversal symmetry, is left. This is demonstrated clearly in Fig. 3(b) where each dispersion curve from Fig. 3(a) is split into two curves of similar behavior. A similar but much smaller effect is found for the conduction-band states as well (not shown).

B. Stark localization of carriers in superlattice minibands

Semiconductor superlattices can be designed and fabricated such that their energy spectra contain minibands of some tens of meV width. Carriers, in these minibands, are free to move along the growth axis and their wave functions are spread over the entire superlattice. In such a system, it is relatively simple to apply an electric field along the SL growth direction, such that the potential drop over one period of the SL is comparable to the width of the minibands. This sets an experimental stage for testing old quantum-mechanical predictions such as Bloch oscillations, the formation of a Stark ladder, and field-induced localization.[25]

The intuitive way to understand the evolution of the system with the application of an external electric field is the following. The SL is a series of coupled QW's, and it is the coupling between the QW's that gives the mini-
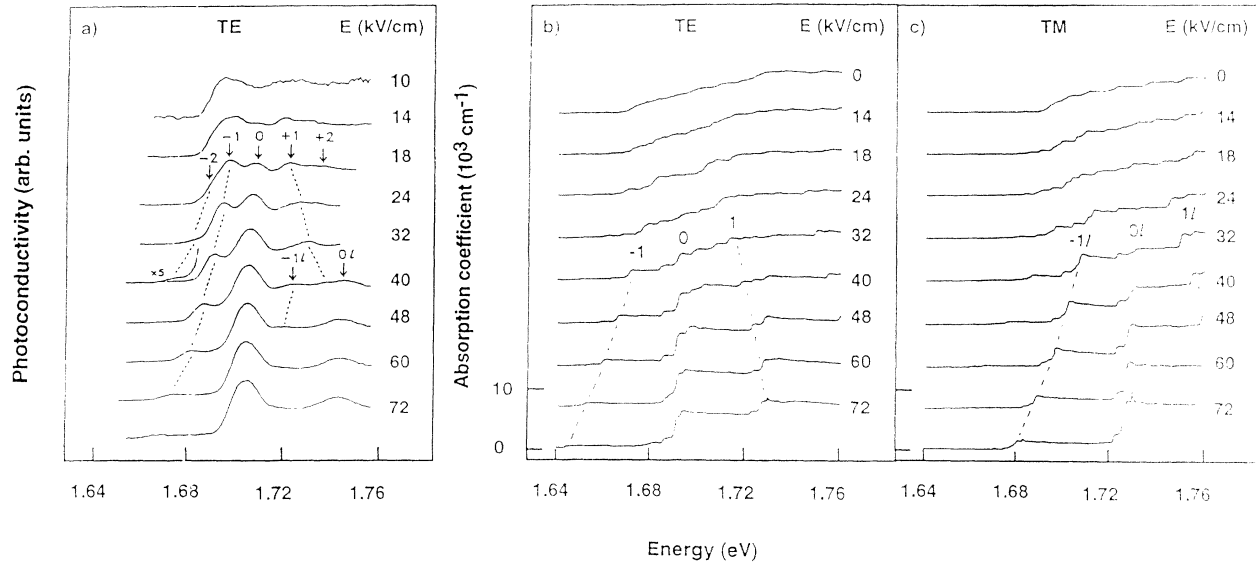
FIG. 4. (a) Measured TE polarized photocurrent spectra of an $Al_xGa_{1-x}As/GaAs$ superlattice subject to various electric fields. The labeled peaks are explained in the text. (After Ref. 28.) (b) and (c) The calculated absorption spectra of the same superlattice subject to the same electric fields for TE and TM polarization, respectively.

bands their widths.[26] The application of an external electric field results in a removal of this coupling, and the genuine energy spectrum of the individual QW's is restored. The energy difference between states localized in adjacent QW's is given by the potential difference between the two QW's. As a result, the spectrum of the entire SL evolves into a ladderlike set of discrete levels and the wave function of carriers in these levels tends to gradually localize over a few adjacent wells. This simple picture was recently checked experimentally by means of photocurrent excitation spectroscopy by Mendez and co-workers.[27] In Fig. 4, we compare their experimental measurements with our model calculation. Figure 4(a) shows the measured photocurrent spectra of a superlattice for various electric fields applied along its growth axis. The spectra, which are taken from Ref. 27, were obtained from measurements performed on a SL imbedded in the intrinsic region of a p-i-n structure. The SL consisted of 60 periods of alternating 30-Å-thick GaAs layers and 35-Å-thick $Al_{0.65}Ga_{0.35}As$ layers. For the measurements, unpolarized light at normal incidence to the layers was used. For comparison we show, in Figs. 4(b) and 4(c), the calculated spectra for light polarized parallel to the layers (TE polarization, like the experiment) and for light polarized parallel to the growth axis (TM polarization), respectively. The input structure to the calculation consisted of seven wells, isolated by high barriers, in a similar way to that illustrated in Fig. 1. Full convergence was reached with five wells in the simulation unit cell, and 49 plane waves in the Fourier expansion of the envelope wave functions. Sixty states were calculated for each in-plane k vector. These calculations were thus somewhat more demanding than the corresponding calculations of the Stark effect in a MQW structure. The photoconductivity spectra, displayed in Fig. 4(a), show a considerable complexity and are quite rich in spectral

features, especially at high electric fields. It is seen both in the experiment and in the simulation that the spectrum, which was originally quite featureless, acquires more structure and identifiable peaks appear as the applied field increases. The peaks evolve with the application of the field, both in intensity and in spectral position. In order to facilitate an easy identification of these spectral features, we use the calculated spectra in the TE polarization [Fig. 4(b)] and in the TM polarization [Fig. 4(c)]. In the TE polarization, the heavy-hole associated optical transitions are roughly a factor of three stronger than the corresponding light-hole associated transitions. In contrast, in the TM polarization the heavy-hole transitions are almost inactive. The use of the polarization selection rules for the interpretation of the measurement is very useful. From inspection of Figs. 4(b) and 4(c) it can be seen that the strong peaks, observed at energies of 1.703 and 1.74 eV when the highest field is applied to the SL, are heavy-hole and light-hole associated transitions, respectively. This is in agreement with the interpretation of the authors of Ref. 27, who marked these peaks as $0(h)$ and $0(l)$, respectively. Indeed, as can be deduced from the inspection of the associated envelope wave functions, these transitions originated from electrons and holes, which are localized in the same QW. Similarly, a detailed comparison between the measured spectrum and the calculated ones, as well as inspection of the calculated envelope wave functions (as shown, for example, in Fig. 5), allows us to unambiguously identify the peaks denoted by -2, -1, $+1$, $+2$, and $-1l$ as well. These peaks correspond to transitions involving electrons with a wave function primarily localized in one well and holes with a wave function primarily localized within wells one or two periods away.

Although there are similarities between the computed and experimental spectra there are also differences. The

GaAs   AlGaAs

144 kV/cm

72 kV/cm

32 kV/cm

0 kV/cm

0   200   400   600   800
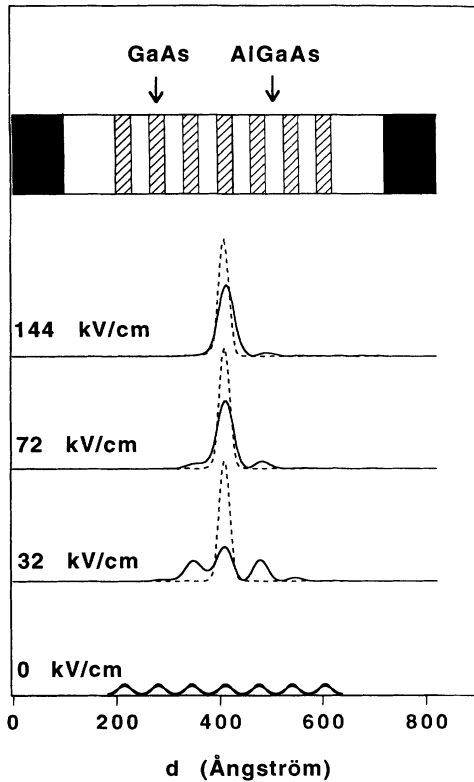
d (Ångström)

FIG. 5. The calculated electron (solid line) and heavy-hole (dashed lines) probability of distribution in a superlattice subject to various applied electric fields. The structure is also shown in the top of the figure, where the black areas represent the artificially high potential isolating barriers.

energy difference between the computed spectra and the experimental spectra is about 10 meV. It can also be noted that while the experiments start to show considerable structure at an electric field of about 28 kV/cm, the computed spectra require an electric field of about 32 kV/cm before well-resolved features appear. We believe that some of these discrepancies can be attributed to the neglect of excitonic effects. Others are the result of the comparison between photocurrent measurements and absorption calculations. One should bear in mind that the photocurrent excitation spectra also include contributions from transport as well as carrier collection efficiency, which may depend on the carrier energy and the field strength. The formation of different electric-field domains, due to screening by residual carriers,[28] may also contribute to the complexity of the experimental data, and some uncertainty in determining the electric-field strength from the voltage on the device. We believe that in a comparison with absorption data, instead of photocurrent data, some of these discrepancies will disappear.

The electric-field-induced localization effect, as calculated by our model, is demonstrated in Fig. 5. In Fig. 5, we display the calculated electron (solid lines) and heavy-hole (dashed lines) probability distribution (absolute magnitude of the envelope wave function squared) at various electric fields. At zero electric field, the wave functions are delocalized and spread over the entire

structure. At a field strength of 32 kV/cm the heavy-hole wave function is completely localized in one well (chosen to be the middle well in the figure), while the electron is only partially localized. This is a consequence of the greater effective mass of the heavy hole. At increasing field strengths, the electron becomes more and more localized. A field of 144 kV/cm is required to localize the electron to one well. At this field, as can be seen in Fig. 5, the heavy-hole and the electron wave functions are localized on opposite sides of the same QW. Thus, the conventional situation of the quantum confined Stark effect in a single QW is restored.

C. The Stark effect on intersubband transitions

Optical transitions between conduction or valence subbands have become the subject of intensive research and engineering efforts. Scientifically, these transitions provide a direct probe into the electron and hole population densities and relaxation processes within their respective subbands. Technologically, they increase the range of the optical response of the conventional III-V heterostructures to longer wavelengths than obtained by interband transitions,[29] and they allow the achievement of significant absorption at long wavelengths from heterostructures of indirect materials such as silicon and germanium.[30] A variety of light detectors and emitters, which use these intersubband transitions, have been proposed and constructed.[31] Optical gain and lasing oscillations in intersubband devices have recently been reported.[32] These devices use electric fields to collect the generated charge carriers and to align the subbands of consecutive QW's. The latter is of utmost importance, since it allows operation in resonant conditions under which transport is efficient and population inversion can be achieved.[32] Our model provides the means to accurately calculate the effect of the electric field on the subband structure and on the optical transitions between these subbands. In fact, the model applies to intersubband transitions as successfully as to interband transitions. We demonstrate this, in this section, by calculating the Stark effect on the inter-sub-conduction-band transitions of an $Al_xGa_{1-x}As/GaAs$ MQW structure. We compare our calculations to the measured results of Harwit and Harris,[8] who demonstrated this effect.

The structure reported on in Ref. 8 consisted of 50, 120-Å-thick GaAs QW's separated by 350-Å-thick barriers of $Al_{0.5}Ga_{0.5}As$. The center 150 Å of each barrier was doped at 5×10^{17} cm^{-3} with silicon impurities. For the calculation we used an input structure, similar to that displayed in Fig. 1, with only one QW in a unit cell. Twenty-seven plane waves were used for the expansion of the envelope wave functions. An electron concentration of 1.12×10^{17} cm^{-3} in each period, and thermal equilibrium at 94 K, was used for the calculations to match the experimental conditions. In Fig. 6(a) the measured intersubband absorption spectra from Ref. 8 are displayed with an electric field of 36 kV/cm (solid line) and without an electric field (dashed line). The calculated spectra are displayed for comparison in Fig. 6(b). The spectra contain one peak with energy width of about 5 meV at half
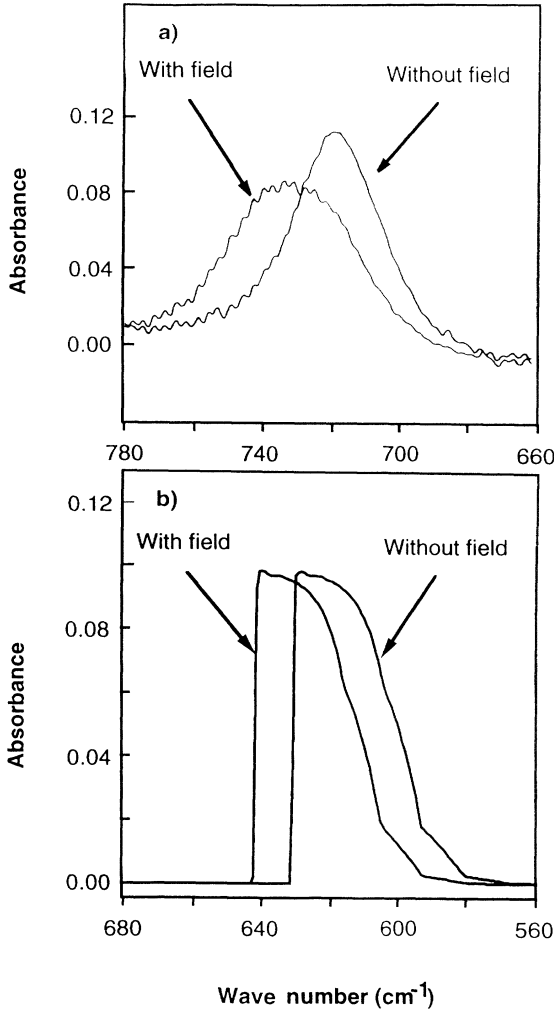
FIG. 6. Measured (a) and calculated (b) inter-sub-conduction-band absorption with and without electric field. The experimental data is after Ref. 8.
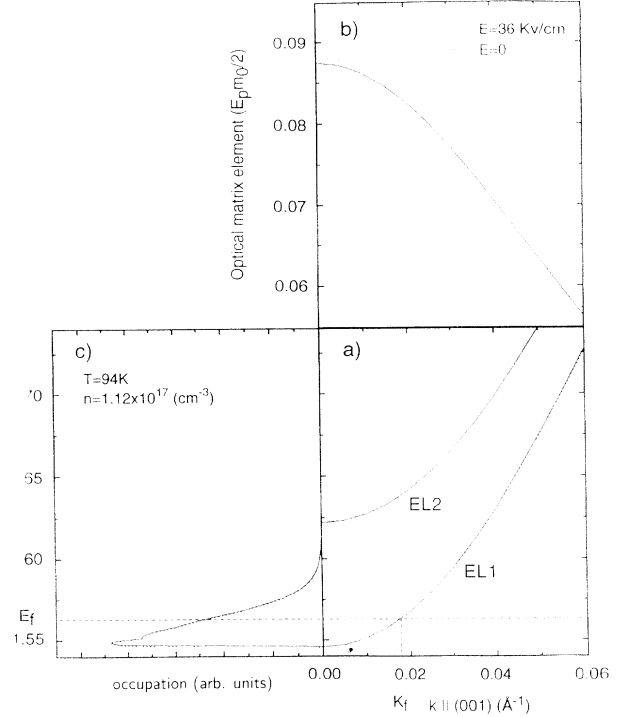

FIG. 7. Calculated in-plane dispersion (a) of the first two conduction subbands of the SL from Ref. 8. The square of the matrix element for optical transitions between them are given in (b) and the occupation numbers are given in (c), where the Fermi energy is indicated by the dashed line. $E_p = 28.8$ eV is the GaAs conduction-valence-band interaction strength.

the maximum. The peak is attributed to the optical transition from the EL1 to the EL2 electron levels in the MQW's. As can be seen in Fig. 6, both the experimental and the computed transitions shift about 1 meV towards higher energy with the applied field. The energy position of the experimental and calculated transitions is, however, different by about 15 meV. This discrepancy can be attributed to an inaccuracy in the determination of the width of the MQW's due to differences between the actual growth rate and the estimated one, as the authors of Ref. 8 themselves suggested. In fact, our calculations of the transition energy agrees well with the calculation done in Ref. 8. Thus, the single-band effective-mass model is quite accurate for the calculations of optical transitions between confined electron levels. The single-band model is not sufficient, however, when transitions between sub-valence-band levels[33] and transitions from confined levels to levels in the continuum[34] are modeled.

The absolute magnitude of the calculated absorption, as well as its spectral width agrees well with the experi-

ment. We show, in Fig. 7, that the low-energy tail of the calculated transition is due to the difference between the effective mass of electrons in the EL1 and the EL2 levels and the thermal distribution of electrons in the EL1 level of the MQW's. It is seen, in Fig. 7, that electrons that occupy states of higher in-plane crystal momentum have lower transition energies and lower optical-matrix elements for the transition. The maximum transition energy is, thus, between EL1 and EL2 states, which have zero crystal momentum. This also explains the sharp edge at the high-energy side of the calculated transitions. The discrepancy between the calculated and measured line shape of the transitions, which is much more symmetric, can be attributed to inhomogeneous line broadening mechanisms (mainly well-width fluctuations[34]), which are not included in the model.

IV. CONCLUSION

We have used the fact that the electric-field operator is diagonal in the k·p approximation (Kane model) to introduce it into an eight-band envelope-function effective Hamiltonian. This Hamiltonian is applicable to semiconductor quantum structures of zero, one, and two dimensions, such as quantum dots, quantum wires, and quantum wells, respectively. In order to test the model and

demonstrate its usefulness, we have applied it to three different cases of electroabsorption: the quantum confined Stark effect in single quantum wells, the Stark effect in a superlattice, and the Stark effect seen in intersubband transitions. The calculations have been compared with published experimental data and found to agree well with the measurements. Most of the differences may be attributed to excitonic effects, which are not included in the model.

*Permanent address: Department of Solid State Physics, Box 118, Lund University, S-221 00 Lund, Sweden.

[1] D. A. B. Miller, D. S. Chemla, T. C. Damen, A. C. Gossard, W. Wiegmann, T. H. Wood, and C. A. Burrus, Phys. Rev. Lett. 53, 2173 (1984).

[2] D. A. B. Miller, D. S. Chemla, T. C. Damen, A. C. Gossard, W. Wiegmann, T. H. Wood, and C. A. Burrus, Phys. Rev. B 32, 1043 (1985).

[3] F. Y. Juang, J. Singh, P. K. Bhattacharya, K. Bajemo, and R. Merlin, Appl. Phys. Lett. 48, 1246 (1986).

[4] H. J. Polland, L. Schultheis, J. Kuhl, E. O. Gobel, and C. W. Tu, Phys. Rev. Lett. 55, 2610 (1985).

[5] Y. J. Chen, E. S. Koteles, B. S. Elman, and C. A. Armiento, Phys. Rev. B 36, 4562 (1987).

[6] H. Temkin, D. Gershoni, and M. B. Panish, Appl. Phys. Lett. 50, 1776 (1987); D. J. Mowbray, M. S. Skolnick, D. Lee, P. A. Claxton, and J. S. Roberts, ibid. 53, 752 (1988).

[7] T. H. Wood, Appl. Phys. Lett. 48, 1413 (1986).

[8] Alex Harwit and J. S. Harris, Jr., Appl. Phys. Lett. 50, 685 (1987).

[9] T. H. Wood, C. A. Burrus, D. A. B. Miller, D. S. Chemla, T. C. Damen, A. C. Gossard, and W. Wiegmann, IEEE J. Quantum Electron. QE-21, 117 (1985); Appl. Phys. Lett. 47, 190 (1985).

[10] T. H. Wood, C. A. Burrus, A. H. Gnauck, J. M. Wiesenfeld, D. A. B. Miller, D. S. Chemla, and T. C. Damen, Appl. Phys. Lett. 47, 190 (1985).

[11] D. A. B. Miller, D. S. Chemla, T. C. Damen, A. C. Gossard, W. Wiegmann, T. H. Wood, and C. A. Burrus, Appl. Phys. Lett. 45, 13 (1984).

[12] F. Capasso, K. Mohamed, and A. Y. Cho, IEEE J. Quantum Electron. QE-22, 1853 (1986).

[13] E. O. Kane, in Handbook on Semiconductors, edited by W. Paul (North-Holland, Amsterdam, 1982), Vol. 1, pp. 193–217.

[14] J. M. Luttinger and W. Kohn, Phys. Rev. 97, 869 (1955).

[15] R. Eppenga, M. F. H. Schuurmans, and S. Colak, Phys. Rev. B 36, 1554 (1987).

[16] G. A. Baraff and D. Gershoni, Phys. Rev. B 43, 4011 (1991).

[17] D. Gershoni, C. H. Henry, and G. A. Baraff, IEEE J. Quantum Electron. QE-29, 2433 (1993).

[18] Thomas B. Bahder, Phys. Rev. B 41, 11 992 (1990).

[19] G. E. Pikus and G. L. Bir, Fiz. Tverd. Tela (Leningrad) 1, 1624 (1959) [Sov. Phys. Solid State 1, 1502 (1960)].

[20] See any text book on quantum mechanics, e.g., J. J. Sakurai, Modern Quantum Mechanics (Addison-Wesley, New York, 1985).

[21] G. D. Sanders and K. K. Bajaj, Phys. Rev. B 35, 2308 (1987).

[22] I. Bar-Joseph, C. Klingshirn, D. A. B. Miller, D. S. Chemla, U. Koren, and B. I. Miller, Appl. Phys. Lett. 50, 1010 (1987).

[23] D. A. B. Miller, J. S. Weiner, and D. S. Chemla, IEEE J. Quantum Electron. QE-22, 1816 (1986).

[24] D. S. Chemla, D. A. B. Miller, P. W. Smith, A. C. Gossard, and W. Wiegmann, IEEE J. Quantum Electron. QE-20, 265 (1984).

[25] G. H. Wannier, Elements of Solid State Theory (Cambridge University Press, Cambridge, England, 1959), pp. 190–193.

[26] J. Bleuse, G. Bastard, and P. Voisin, Phys. Rev. Lett. 60, 220 (1988).

[27] E. E. Mendez, F. Agulló-Rueda, and J. M. Hong, Phys. Rev. Lett. 60, 2426 (1988).

[28] R. E. Cavvichi, D. V. Lang, D. Gershoni, A. M. Sergent, H. Temkin, and M. B. Panish, Phys. Rev. B 38, 13 474 (1988).

[29] C. West and S. J. Eglash, Appl. Phys. Lett. 46, 1156 (1985).

[30] R. P. G. Karunasiri, J. S. Park, and K. L. Wang, Appl. Phys. Lett. 59, 2588 (1991).

[31] B. F. Levine, J. Appl. Phys. 74, R1 (1993).

[32] J. Faist, F. Capasso, C. Sirtori, D. L. Sivco, A. L. Hutchinson, S-N. G. Chu, and A. Y. Cho, Electron. Lett. 29, 2230 (1993).

[33] Y. C. Chang and R. B. James, Phys. Rev. B 39, 12 672 (1989).

[34] D. Gershoni, J. Oiknine-Schlesinger, E. Ehrenfreund, D. Ritter, R. A. Hamm, and M. B. Panish, Phys. Rev. Lett. 71, 2975 (1993).